Nuclear Instruments and Methods in Physics Research B 303 (2013) 62–67

Contents lists available at SciVerse ScienceDirect

Nuclear Instruments and Methods in Physics Research B

journal homepage: www.elsevier.com/locate/nimb

Phase-field simulations of intragranular fission gas bubble evolution in UO_2 under post-irradiation thermal annealing

Yulan Li, Shenyang Hu *, Robert Montgomery, Fei Gao, Xin Sun

Pacific Northwest National Laboratory, 902 Battelle Blvd., Richland, WA 99352, USA

ARTICLE INFO

Article history:
Received 13 July 2012
Received in revised form 20 November 2012
Accepted 21 November 2012
Available online 2 January 2013

Keywords:
Phase-field approach
Intragranular gas bubble evolution
Post-irradiation annealing
UO_2

ABSTRACT

Fission gas bubbles are one of the evolving microstructures that affect thermal mechanical properties, such as thermal conductivity, gas release, volume swelling, and cracking, in operating nuclear fuels. Therefore, fundamental understanding of gas bubble evolution kinetics is essential to predict the thermodynamic property and performance changes of fuels. In this work, a generic phase-field model was developed to describe the evolution kinetics of intragranular fission gas bubbles in UO_2 fuels under post-irradiation thermal annealing conditions. Free energy functional and model parameters are evaluated from atomistic simulations and experiments. Critical nucleus size of gas bubbles and gas bubble evolution were simulated. A linear relationship between logarithmic bubble number density and logarithmic mean bubble diameter was predicted, which is in good agreement with experimental data.

Published by Elsevier B.V.

1. Introduction

During irradiation of light water reactor (LWR) fuel, the fission process generates many different fission product atoms, including xenon (Xe) and krypton (Kr) atoms. The noble gas atoms Xe and Kr represent about 30% of the fission products produced, and the gas atoms' behavior is important to the microstructure evolution and overall performance of the fuel, such as fission gas release to the fuel rod environment and volumetric swelling. Because of the extremely low solubility of the noble gas atoms in the UO_2 matrix, gas bubbles composed of Xe, Kr, and other gas atoms precipitate into gas bubbles. For more than 50 years, the behavior of fission gas atoms in UO_2 has been extensively studied using experiments performed on single-crystal and polycrystalline materials under a variety of temperature and irradiation conditions [1–7]. From these studies, a general picture of the mechanisms that influence the transport and release of fission gas atoms and gas bubble evolution has been developed. Thermally induced fission gas diffusion and release from the fuel generally occurs in two stages: (1) diffusion and trapping of single Xe gas atoms within the grains and (2) formation and interlinkage of grain boundary bubbles. Therefore, intragranular gas bubble evolution kinetics and their effect on bulk diffusion of Xe gas atoms are essential toward understanding the gas release.

Gas bubble nucleation and growth require continuous supplies of both vacancies and gas atoms. Starvation of either vacancies or gas atoms will limit the bubble growth. Due to the high pressure inside of gas bubbles and the large lattice mismatch of interstitial Xe atoms and U vacancies, elastic interaction can be an important driving force or resistance for the diffusion of vacancies and Xe atoms. Defects, such as dislocations, are "sinks," or sources of vacancies. The spatial distribution and density of dislocations affect the sink, or emission strength of vacancies, as well as the concentration of vacancies. Therefore, gas bubble evolution is a complex thermodynamic and kinetic process. In this work, a generic phase-field model is developed to describe the intragranular gas bubble evolution and parametrically investigate the effect of thermodynamic and kinetic properties on gas bubble evolution kinetics. The simulation results for post-irradiation thermal annealing are validated by experimental results.

2. Phase-field model of fission gas bubble evolution in UO_2

To simplify the complicated process without losing the main physics, we made the following assumptions:

(1) Xe atoms may occupy U vacancy lattices or interstitial lattices that depend on valid U vacancy concentration and Xe concentration. For the simplicity of description, the Xe_U (Xe occupies one uranium vacancy) is described by a cluster of a U vacancy and an interstitial Xe atom. Thus, Xe concentrations in U lattices and interstitial lattices can be described by one concentration: gas concentration. Such a two-sublattice model (host and interstitial lattices) allows one (i) to describe the gas bubble with different ratio of vacancies

* Corresponding author.
E-mail address: shenyang.hu@pnnl.gov (S. Hu).

0168-583X/$ - see front matter Published by Elsevier B.V.
http://dx.doi.org/10.1016/j.nimb.2012.11.028

and Xe atoms based on the equation of state of gas phase; (ii) to study the effect of vacancy and Xe mobility on gas bubble evolution; and (iii) to study the effects of starvation and vacancy emission on gas bubble growth.

(2) Xe interstitial, U vacancy, and the Xe_U (Xe occupies one uranium vacancy) have very different mobility from the calculation of migration energy of defects [8,9]. In addition, other complexes, such as Xe_{UO} (Xe occupies one uranium vacancy and one oxygen vacancy) and Xe_{UO2} (Xe occupies one uranium vacancy and two oxygen vacancies), also contribute to the diffusion of vacancies and Xe atoms. Hence, the effective mobility of U vacancies and Xe atoms is used in the model. In the present simulations, an effective migration energy of 3.9 eV is used for both U vacancy and Xe atom. However, the model has no limitation in using different mobility of U vacancies and Xe atoms. If a Xe atom stays in an interstitial position it may diffuse with a rather low barrier (1.6 eV) compared to vacancy diffusion. Even so, such assumption of same mobility should not affect the evolution kinetics of bubbles because that is controlled by the one having lower mobility.

(3) Gas bubbles formed at low temperature may be unstable at the annealing temperature. Thus, initial size distribution of gas bubbles may dramatically impact the results of gas bubble number and size evolution. In the current simulations, a normal (Gaussian) distribution with a mean radius of ~1 nm and standard deviation of 0.5 nm is used to generate the initial gas bubble size distribution.

(4) Chemical potential gradient is one driving force for vacancy and Xe diffusion. We use Kim's model [10] to describe the chemical free energy of matrix and gas phases. To efficiently solve the phase-field evolution equations, two parabolic functions are used to fit the ideal solution free energy of the matrix with vacancies and Xe atoms and the free energy of the gas bubble phase, calculated from the equation of state.

(5) Dislocations are sinks or sources of vacancies. Because of the lack of sink and emission strengths, the emission rate of vacancies from dislocations is taken as a model parameter, like the initial vacancy concentration.

(6) Experiments [2] suggest that vacancy emission could be an important mechanism that affects gas bubble evolution kinetics. Therefore, we assumed that initial vacancy concentration is a model parameter.

(7) O vacancy has much higher mobility than U vacancy and the Xe atom. However, it is not a rate-limiting species in gas bubble growth. Therefore, we neglected O vacancies. Its effect is accounted in to the effective diffusivity of U vacancies and Xe atoms.

(8) The contribution of small gas bubble migration at high temperature to gas bubble evolution is ignored in this model. However, a phase-field model of void migration can be extended to describe gas bubble migration [11,12].

In the phase-field modeling framework, the microstructure of intragranular fission gas bubbles in UO_2 can be described by two sets of field variables. One is the concentration variables describing the concentrations of diffusive vacancies and gas atoms. The other is the order parameter distinguishing the matrix and gas phases. In reality, there are a number of mobile vacancies in irradiated UO_2, such as single O and U vacancies and small vacancy clusters. The fission reaction also produces a number of fission gas atoms, including Xe, Kr, and He, which form the gas phase. For simplicity, we use variable $c_v(\mathbf{r},t)$ to describe the overall vacancy concentration, which includes O and U vacancies and their vacancy clusters, and $c_g(\mathbf{r},t)$ to describe overall gas atoms (Xe, Kr, He, etc.) concentration. $\mathbf{r}$ and t are the spatial coordinate and time, respectively. We assume that vacancies and gas atoms diffuse with effective diffusivity. Thus, two sublattices, i.e., the host and interstitial lattice, are used to describe the crystal structure. The host lattice is occupied by the U or O atom or vacancy, while gas atoms occupy the interstitial lattices. The $c_v(\mathbf{r},t)$ and $c_g(\mathbf{r},t)$ are the numbers of moles in the molar volume of UO_2 lattices, respectively. Here, we imply the ratio of U and O vacancies in the molar volume remains 1:2 during the absorption, emission, and diffusion processes. The order parameter is denoted by $\eta(\mathbf{r},t)$, which is 1 in the gas bubble phase and 0 in the matrix phase. Across the interface between a gas bubble and the matrix, $\eta(\mathbf{r},t)$ smoothly varies from 1 to 0.

The total free energy of the system includes the chemical free energy, gradient energy, and long-range interaction energy and is written as a function of the phase-field variables as:

$$E=\int_V\left[F(c_v,c_g,\eta,T)+\frac{\kappa^2}{2}|\nabla\eta|^2+U^{def}(\varepsilon_{ij})\right]dV, \tag{1}$$

where V is the system volume; $F(c_v,c_g,\eta,T)$ is the chemical free energy density; T is absolute temperature; κ is the gradient coefficient associated with interfacial energy of gas bubbles; U^{def} is the elastic energy density associated with the lattice mismatch of the defects, including distributed gas bubbles, vacancies, and gas atoms; and ε_{ij} $(i,j=1,2,3)$ are total strain components.

Following Kim's solidification model [10], the chemical free energy density of the system is constructed as:

$$F(c_v,c_g,\eta,T)=[1-h(\eta)]f^m(c_v^m,c_g^m,T)+h(\eta)f^b(c_v^b,c_g^b,T)+wg(\eta) \tag{2}$$

where (f^m,f^b), (c_v^m,c_g^m), and (c_v^b,c_g^b) are the chemical free energy densities, vacancy and gas concentrations of the matrix (m) and gas bubble (b) phases, respectively. $g(\eta)$ is a double-well potential. For example, the simplest form is $g(\eta)=\eta^2(1-\eta)^2$, and w is the height of the double-well potential. $h(\eta)=3\eta^2-2\eta^3$ is an interpolation function that describes the volume fraction of the gas bubble phase. Kim's model assumes that any point within the interface region is considered a mixture of the matrix and gas bubble phases with the same interdiffusion potential. Therefore, the concentrations satisfy the following chemical equilibrium and mass balance equations:

$$c_v=[1-h(\eta)]c_v^m+h(\eta)c_v^b \tag{3a}$$

$$c_g=[1-h(\eta)]c_g^m+h(\eta)c_g^b \tag{3b}$$

$$\frac{\partial f^m(c_v^m,c_g^m,T)}{\partial c_v^m}=\frac{\partial f^b(c_v^b,c_g^b,T)}{\partial c_v^b} \tag{3c}$$

$$\frac{\partial f^m(c_v^m,c_g^m,T)}{\partial c_g^m}=\frac{\partial f^b(c_v^b,c_g^b,T)}{\partial c_g^b}. \tag{3d}$$

From Eqs. (3a)–(3d), we can obtain (c_v^m,c_g^m) and (c_v^b,c_g^b) for a given (c_v,c_g).

With the ideal solution assumption, the chemical free energy density of the matrix phase with vacancy and gas concentration $c_v(\mathbf{r},t)$ and $c_g(\mathbf{r},t)$ can be written as:

$$f^m(c_v^m,c_g^m,T)=\frac{1}{\Omega}\Big\{\Re T[c_v^m\ln(c_v^m)+(1-c_v^m)\ln(1-c_v^m)]+N_AE_v^fc_v^m+\Re T[c_g^m\ln(c_g^m)+(1-c_g^m)\ln(1-c_g^m)]+N_AE_g^fc_g^m\Big\}, \tag{4}$$

where $\Re=8.314$ [J/(mol·K)] is the gas constant, and $N_A=6.022\times10^{23}[\mathrm{mol}^{-1}]$ is the Avogadro constant. E_v^f and E_g^f are the formation energies of a vacancy and a gas atom, respectively.

Ω is the molar volume of UO_2, and $\Omega = 2.53 \times 10^{-5}$ [m^3/mol] is used.

In simulations, $f^m(c_v^m, c_g^m, T)$ is replaced approximately by parabolic functions as:

$$f^m(c_v^m, c_g^m, T) = A_{12}(c_v^m - c_v^{m,eq})^2 + B_{12}(c_g^m - c_g^{m,eq})^2, \quad (5)$$

where $c_v^{m,eq} = \exp(-E_v^f/k_BT)$ and $c_g^{m,eq} = \exp(-E_g^f/k_BT)$ are the thermal equilibrium solubility of vacancies and gas atoms, respectively. $k_B = 1.381 \times 10^{-23}$ [J/K] is the Boltzmann constant. Both $f^m(c_v^m, c_g^m, T)$ in Eqs. (4) and (5) have the same first derivatives at a given concentration (c_v^0, c_g^0). If assuming a UO_2 vacancy has the same formation energy as a Xe atom, $E_v^f = E_g^f = E^f = 3$ eV. In the following simulations, $(c_v^0, c_g^0) = (0.01, 0.01)$, $B_{12} = A_{12}$, and $\frac{A_{12}}{C_{44}} = \frac{-a_2+3a_1}{4(c_v^0 - c_v^{m,eq})} + \frac{a_2 - a_1}{2400(c_v^0 - c_v^{m,eq})} T$:

$$a_1 = 0.178605 - 0.0030782\log(1 - c_v^0) + 0.0030782\log(c_v^0)$$

$$a_2 = 0.178605 - 0.00923461\log(1 - c_v^0) + 0.00923461\log(c_v^0)$$

with $C_{44} = 64$ [GPa] [13].

For added simplicity, the chemical free energy density of the gas bubble phase is assumed to be parabolic functions of c_v^b and c_g^b as:

$$f^b(c_v^b, c_g^b, T) = A_{22}(c_v^b)^2 + A_{21}c_v^b + A_{20} + B_{22}(c_g^b)^2 + B_{21}c_g^b + B_{20}. \quad (6)$$

If $c_v^{b,eq}$ and $c_g^{b,eq}$ are the equilibrium concentrations of the gas bubble phase, $c_v^{b,eq} = 1$ and $c_g^{b,eq}$ can be obtained from the equation of state of Xe. We used Ronchi's Xe results [14] to determine the equilibrium gas concentration $c_g^{b,eq} \approx 0.7$, which corresponds to 2 GPa internal pressure in the gas bubbles. The two remaining unknown coefficients (e.g., A_{22} and B_{22}) will be determined by given $(c_v^{cross}, c_g^{cross}; f^{cross})$, i.e., $f^m(c_v^{cross}, c_g^{cross}, T) = f^b(c_v^{cross}, c_g^{cross}, T) = f^{cross}$. Therefore,

$$A_{22} = \frac{A_{12}f^{cross}}{(\sqrt{A_{12}}(c_v^{m,eq} - c_v^{b,eq}) + \sqrt{f^{cross}})^2},$$

$$B_{22} = \frac{B_{12}f^{cross}}{(\sqrt{B_{12}}(c_g^{m,eq} - c_g^{b,eq}) + \sqrt{f^{cross}})^2}.$$

In the following simulation, $f^{cross}/C_{44} = 0.5$ is used. The corresponding chemical free energy is demonstrated by Fig. 1.

The last term of the right side of Eq. (1) is the elastic energy. If we assume the variation of stress-free lattice parameter of the matrix phase, a, with the given concentrations of vacancies and gas atoms obeys Vegard's law, the local stress-free strain caused by the defect inhomogeneity is given by:

$$\varepsilon_{ij}^{*m} = [\varepsilon^{v0}(c_v - c_v^{m,eq})\delta_{ij} + \varepsilon^{g0}(c_g - c_g^{m,eq})\delta_{ij}](1 - h(\eta)) \quad (7)$$

where $\varepsilon^{v0} = (1/a)da/dc_v$ and $\varepsilon^{g0} = (1/a)da/dc_g$ are the expansion coefficients of the lattice parameter due to the introduction of vacancies and interstitials, respectively, and δ_{ij} is the Kronecker delta function. The vacancy and gas concentrations are high in the gas bubble phase, where Vegard's law may no longer be applicable. The stress-free strain in the gas bubble phase is described as:

$$\varepsilon_{ij}^{*b}(\mathbf{r}) = \varepsilon^{b0}(c_g, T)\delta_{ij}h(\eta) \quad (8)$$

where $\varepsilon^{b0}(c_g, T)$ can be estimated as $\varepsilon^{b0}(c_g, T) = P/(C_{11} + 2C_{12})$ and P is the pressure inside of the gas bubble phase that can be obtained from the equation of state, and C_{11} and C_{12} are the elastic constants of the gas bubble phase. Thus, the total stress-free strain tensor is:

$$\begin{aligned}\varepsilon_{ij}^* &= \varepsilon_{ij}^{*m} + \varepsilon_{ij}^{*b} \\ &= [\varepsilon^{v0}(c_v - c_v^{m,eq})\delta_{ij} + \varepsilon^{g0}(c_g - c_g^{m,eq})\delta_{ij}][1 - h(\eta)] + \varepsilon^{b0}(c_g, T)\delta_{ij}h(\eta).\end{aligned} \quad (9)$$

The elastic energy density U^{def} is calculated by:

$$U^{def} = \frac{1}{2}\lambda_{ijkl}\varepsilon_{kl}^{el} \quad (10)$$

where the summation convention over the repeated indexes is used. λ_{ijkl} is the elastic constant tensor of the system (its Voigt notation is C_{ij}). ε_{ij}^{el} is the elastic strain, calculated by:

$$\varepsilon_{ij}^{el} = \bar{\varepsilon}_{ij} + \delta\varepsilon_{ij}(\mathbf{r}) - \varepsilon_{ij}^*(\mathbf{r}) \quad (11)$$

where $\bar{\varepsilon}_{ij}$ is the homogeneous strain characterizing the macroscopic shape and volume change and $\delta\varepsilon_{ij}(\mathbf{r})$ is the heterogeneous strain of $\int_V \delta\varepsilon_{ij}(\mathbf{r})dV = 0$. For elastic inhomogeneous solids, such as the UO_2 matrix with voids and gas bubbles, the elastic solution can be obtained using iteration methods [15]. For simplicity, we assume the gas phase has the same elastic constants as UO_2 and of cubic anisotropy with $C_{11}/C_{44} = 6.17$, $C_{12}/C_{44} = 1.89$ [13].

The evolution equations of c_v, c_g, and η are described by the Cahn–Hilliard equation [16] and the Allen–Cahn equation [17] as:

$$\frac{\partial c_v}{\partial t} = \nabla \cdot \left\{ M_{vv}\nabla\left(\frac{\partial(F + U^{def})}{\partial c_v}\right)\right\} + \dot{\omega}(\rho_{dis}, c_v, \sigma_{ij}), \quad (12)$$

$$\frac{\partial c_g}{\partial t} = \nabla \cdot \left\{ M_{gg}\nabla\left(\frac{\partial(F + U^{def})}{\delta c_g}\right)\right\}, \quad (13)$$

$$\begin{aligned}\frac{\partial\eta}{\partial t} &= -L\frac{\delta E}{\delta\eta} = -L\left(\frac{\partial F}{\partial\eta} + \frac{\partial U^{def}}{\partial\eta} - \kappa^2\nabla^2\eta\right) \\ &= -L\Big\{-\kappa^2\nabla^2\eta + wg'(\eta) + h'(\eta)\Big[-(f^m - f^b) + (c_v^m - c_v^g)\frac{\partial f^m}{\partial c_v^m} \\ &\quad + (c_g^m - c_g^g)\frac{\partial f^m}{\partial c_g^m}\Big] + \frac{\partial U^{def}}{\partial\eta}\Big\},\end{aligned} \quad (14)$$

where M_{vv} and M_{gg} represent the mobility of vacancies and gas atoms and are determined from the diffusivity by $M_{vv} = D/(\frac{\partial^2 f^m}{\partial c_v^2})|_{c_v = c_v^{m,eq}}$ and $M_{gg} = D/(\frac{\partial^2 f^m}{\partial c_g^2})|_{c_g = c_g^{m,eq}}$. L is the interface mobility coefficient. $\dot{\omega}(\rho_{dis}, c_v, \sigma_{ij})$ is the vacancy emission rate, which depends on dislocations ρ_{dis}, local stress σ_{ij}, and vacancy concentration $c_v(\mathbf{r}, t)$.

In Kim's model, the interfacial energy γ and interface thickness 2λ are associated with the gradient coefficient κ and the height w of the double-well potential as:

$$\gamma = \frac{k\sqrt{w}}{3\sqrt{2}}, \text{ and} \quad (15)$$

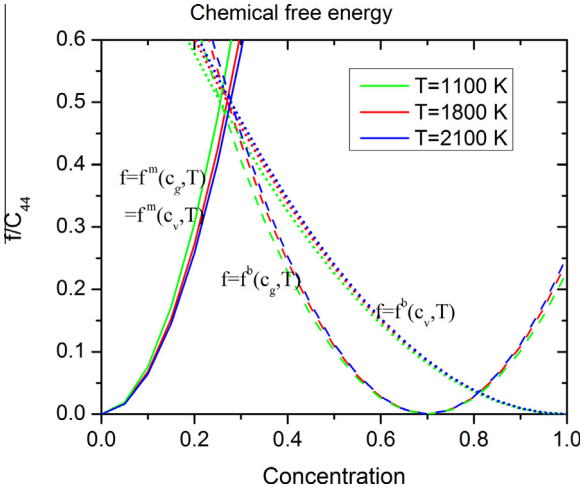

Fig. 1. Chemical free energies versus concentration used in our simulations. The three line colors indicate different temperatures of 1100 K, 1800 K, and 2100 K, respectively. The three line types indicate the different functions of $f^m(c_g, T) = f^m(c_v, T)$, $f^b(c_g, T)$, and $f^b(c_v, T)$, respectively.

$$2\lambda = \alpha\sqrt{2}\frac{\kappa}{\sqrt{w}}, \tag{16}$$

where α is a dimensionless coefficient and takes value of ~2.2.

3. Simulation results and analysis

3.1. Evaluation of the thermodynamic model by testing the critical nucleus sizes of gas bubbles

Based on classical nucleation theory, chemical free energy, elastic energy, and interfacial energy together determine the critical nucleus size of gas bubbles. Before we simulate gas bubble growth kinetics, we first evaluate the effect of concentration and elastic interaction on the critical size of gas bubbles. In the simulations, a gas bubble with different sizes was embedded in the center of a three-dimensional (3D) simulation cell $96dx \times 96dy \times 96dz$. Periodic boundary conditions in x-, y-, and z-directions were imposed. Grid size $dx = dy = dz = 0.25$ nm was used. The simulation was performed at 2100 K. The evolution of gas bubble radius versus time is plotted in Fig. 2(a). The initial vacancy concentration and Xe concentration in the matrix were expressed with the same value. In Fig. 2(a), it is apparent that when the radius of a gas bubble is less than 0.4 nm, the gas bubble shrinks for the studied four cases with different vacancy and Xe concentrations in the matrix and with/without elastic interaction. When the radius of a gas bubble is larger than 0.6 nm, the gas bubble grows in each of the studied four cases. Gas bubbles with a radius between 0.4 nm and 0.6 nm may grow or shrink depending on the concentration and elastic interaction. Therefore, the critical size of gas bubble is about 0.6 nm for the given free energy, interfacial energy, and elastic interaction energy. The critical size increases with decreasing vacancy and Xe concentrations. Fig. 2(b) depicts pressure and shear stress distributions on the x–y plane, which crosses the center of the gas bubble. We found the pressure inside the gas bubble is about 1.6 GPa and is consistent with the equation of state. In addition, the pressure inside the gas bubble causes a long-range elastic field near the gas bubble, which affects gas bubble growth kinetics, as well as the critical size of gas bubbles. The results in Fig. 2(a) shows that the elastic interaction increases the critical size of a gas bubble.

3.2. Gas bubble evolution kinetics in 3D during annealing from 1100 K to 2100 K

Gas bubble evolution kinetics during thermal annealing was simulated in 3D. The simulation started with a random gas bubble distribution with an initial density of $\rho = 9.0 \times 10^{23}/m^3$ in a $128dx \times 128dy \times 36dz$ simulation cell. Here we would point out that because of the advantage of Kim's model which allows one to adjust the double well height to change the interface thickness without affecting the interfacial energy and mobility [10], we can adjust the grid size to simulate physical domain and time in different scale for the given thermodynamic and kinetic properties of a system. With Kim's model, we were able to use small grid size to capture small microstructure such as gas bubble nucleus with high accuracy in the last section. We also can use a larger gird size to capture the microstructure evolution in a larger physical domain and a longer time period in simulations. In our simulations of gas bubble growth, a larger grid size $dx = dy = dz = 1$ nm was used. The initial gas and vacancy concentrations were the same: 0.0042. The annealing started from 1100 K, and temperature increased at a rate of 2 K/s. Several simulations with different initial gas bubble mean sizes and spatial distributions were run. In these simulations, the elastic interaction and vacancy emission from dislocation initially are ignored. Fig. 3 presents the snapshots of temporal evolution of gas bubbles. As expected, the gas bubbles have spherical shapes due to the isotropic interfacial energy. In the beginning, some gas bubbles grow then later shrink during coarsening. When compared, Fig. 3(a and b) and Fig. 3(c and d) illustrate that gas bubble evolution in Fig. 3(a and b) at lower temperature is much slower than that of Fig. 3(c and d) at higher temperature. The number and size evolution of gas bubbles is analyzed. Fig. 4 plots the evolution of both the gas bubble number and gas bubble average diameter. A nearly linear relationship between the logarithmic gas bubble density and logarithmic mean gas bubble diameter exists for different initial mean sizes.

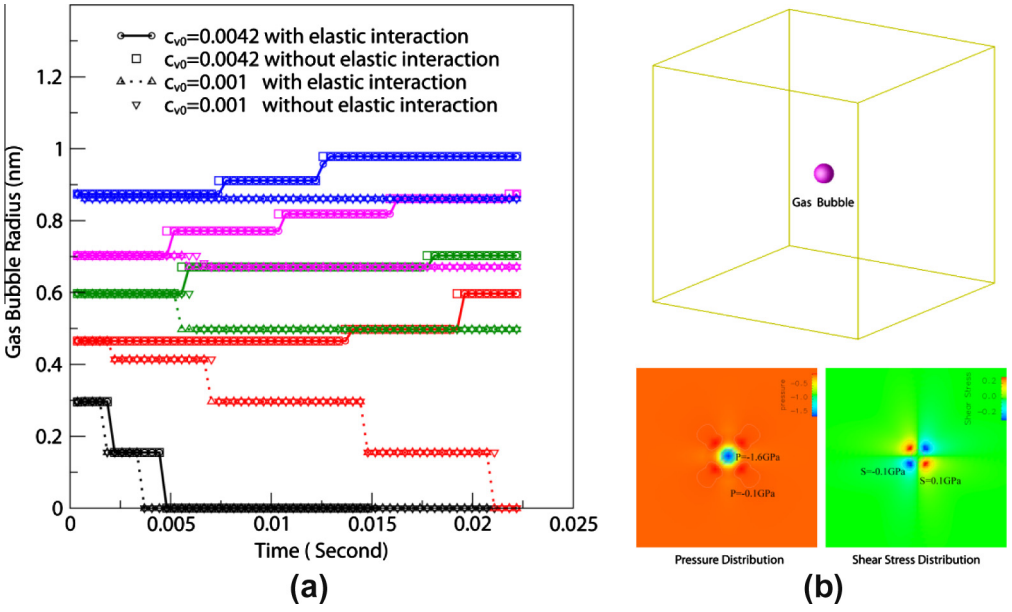

Fig. 2. (a) Concentration and elastic interaction dependence of gas bubble critical size where the colors represent the different initial radii of the gas bubbles, respectively. The initial radius can be identified at 0 s. For each initial radius the four scenarios as illustrated by the different symbols in the legend were simulated. (b) Pressure and shear stress around the gas bubble.

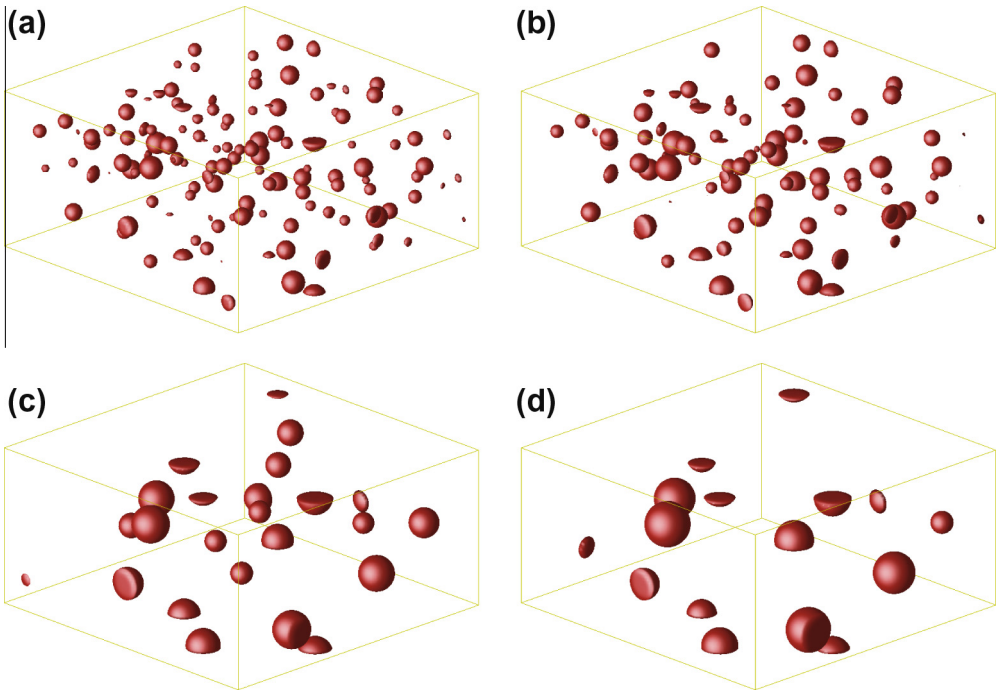

Fig. 3. Gas bubble morphology evolution snapshots: (a) T = 1300 K, t = 150 s; (b) T = 1900 K, t = 427 s; (c) T = 1900 K, t = 450 s; and (d) T = 2000 K, t = 481 s.

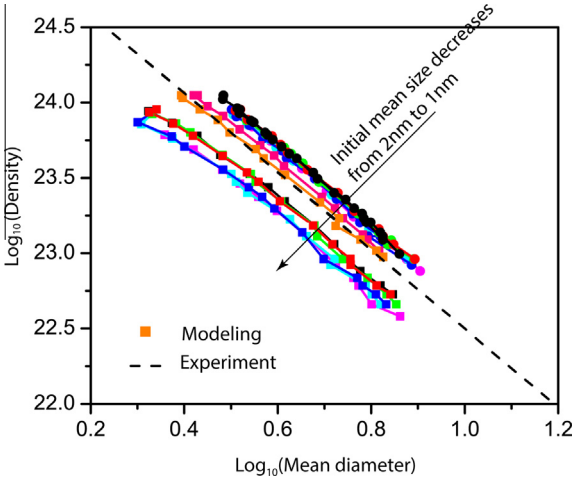

Fig. 4. Gas bubble density versus mean diameters and comparison between simulations and experiments. Simulation results from different initial mean sizes (radii) are indicated by scattered lines.

Kashibe et al. [4] studied experimentally the intragranular gas bubble evolution kinetics during post-irradiation. They found a linear relationship of $\log_{10}N_b \propto -2.6\log_{10}d_b$, where N_b is the bubble density per cubic meter volume and d_b is the mean bubble diameter. Here, we should mention that in the simulations, the same initial gas bubble density and similar mean sizes are used as those observed in the experiment. For comparison, the experimental results also were plotted with a dash line in Fig. 4, indicating that the simulation results agree well with the experimental observation.

The effect of elastic interaction and vacancy emission from dislocations also were simulated. The elastic interaction slows down gas bubble evolution kinetics. Gas bubbles near dislocations grow faster due to the continuous supply of vacancies from dislocations. This may explain the experimental observation that the bubble size distribution exhibits long exponential tails, where the largest bubbles are present in concentrations of 10^4 or 10^5 lower than the concentrations of average-sized bubbles [2]. The effect of thermodynamic and kinetic properties on gas bubble evolution kinetics will be presented in our future work.

4. Summary

We developed a generic phase-field model for simulating intragranular bubble evolution during post-irradiation annealing in UO_2. The thermodynamic properties used in the simulations, including chemical free energy, elastic energy, and interfacial energy, produce a reasonable critical nucleus size of gas bubbles. The predicted intragranular gas bubble evolution kinetics ($\log_{10}N_b \propto -2.6\log_{10}d_b$) is in good agreement with experimental results, suggesting that the model can be used to study parametrically thermodynamic and kinetic properties, such as initial defect concentrations, vacancy emission, elastic interaction, and defect mobility, on gas bubble evolution kinetics.

Acknowledgements

This research was supported by the US Department of Energy's (DOE), Nuclear Energy Advanced Modeling and Simulation (NEAMS) program at Pacific Northwest National Laboratory (PNNL). PNNL is operated by Battelle for the DOE under Contract No. DE-AC05-76RL01830. The authors also would like to thank their collaborators for helpful discussions and suggestions, including Drs. Michael Tonks, Bulent Biner, and Paul Millett at Idaho National Laboratory; Dr. David Andersson at Los Alamos National Laboratory; Dr. Veena Tikare at Sandia National Laboratories; and Dr. Balasubramaniam Radhakrishnan at Oak Ridge National Laboratory.

References

[1] D.R. Olander, D. Wongsawaeng, Re-solution of fission gas – a review: part 1. Intragranular bubbles, J. Nucl. Mater. 354 (2006) 94–109.
[2] R.J. White, The growth of intra-granular bubbles in post-irradiation annealed UO_2 fuel, in: IAEA Technical Committee on Nuclear Fuel Behaviour Modeling at High Burn-up and its Experimental Support Lake Windermere, UK, 2000.

[3] M.E. Cunningham, M.D. Freshley, D.D. Lanning, Fission-gas release during power bumping at high burnup, J. Nucl. Mater. 200 (1993) 24–40.
[4] S. Kashibe, K. Une, K. Nogita, Formation and growth of intragranular fission-gas bubbles in UO_2 fuels with burnup of 6–83 GWD/T, J. Nucl. Mater. 206 (1993) 22–34.
[5] C. Baker, Migration of intra-granular fission-gas bubbles in irradiated uranium–dioxide, J. Nucl. Mater. 71 (1977) 117–123.
[6] J.M. Griesmeyer, N.M. Ghoniem, Response of fission-gas bubbles to the dynamic behavior of point-defects, J. Nucl. Mater. 80 (1979) 88–101.
[7] D.A. Macinnes, I.R. Brearley, A model for the release of fission-gas from reactor-fuel undergoing transient heating, J. Nucl. Mater. 107 (1982) 123–132.
[8] B. Dorado, D.A. Andersson, C.R. Stanek, M. Bertolus, B.P. Uberuaga, G. Martin, M. Freyss, P. Garcia, First-principles calculations of uranium diffusion in uranium dioxide, Phys. Rev. B 86 (2012) 035110.
[9] X.Y. Liu, D.A. Andersson, B.P. Uberuaga, First-principles DFT modeling of nuclear fuel materials, J. Mater. Sci. 47 (2012) 7367–7384.
[10] S.G. Kim, W.T. Kim, T. Suzuki, Phase-field model for binary alloys, Phys. Rev. E 60 (1999) 7186–7197.
[11] S.Y. Hu, C.H. Henager, Phase-field simulation of void migration in a temperature gradient, Acta Mater. 58 (2010) 3230–3237.
[12] Y.L. Li, S.Y. Hu, X. Sun, F. Gao, C.H. Henager, M. Khaleel, Phase-field modeling of void migration and growth kinetics in materials under irradiation and temperature field, J. Nucl. Mater. 407 (2010) 119–125.
[13] J.B. Wachtman, M.L. Wheat, H.J. Anderson, J.L. Bates, Elastic constants of single crystal UO_2 at 25 degrees C, J. Nucl. Mater. 16 (1965) 39–41.
[14] C. Ronchi, Extrapolated equation of state for rare-gases at high-temperatures and densities, J. Nucl. Mater. 96 (1981) 314–328.
[15] S.Y. Hu, L.Q. Chen, A phase-field model for evolving microstructures with strong elastic inhomogeneity, Acta Mater. 49 (2001) 1879–1890.
[16] J.W. Cahn, On spinodal decomposition, Acta Metall. 9 (1961) 795–801.
[17] J.W. Cahn, S.M. Allen, A microscopic theory of domain wall motion and its experimental verification in Fe–Al alloy domain growth kinetics, Le J. de Phys. Col. 38 (1977) 51.